PRECISE ORBIT PROPAGATION FOR SPACE DEBRIS OBJECTS USING THE HERMITE INTEGRATION SCHEME

J. Rodmann, D. Hampf, T. Hasenohr, L. Humbert, W. Riede, F. Sproll, and P. Wagner

German Aerospace Center (DLR), Institute of Technical Physics, 70569 Stuttgart, Germany, Email: jens.rodmann@dlr.de

ABSTRACT

We present a numerical integration technique based on the Hermite scheme, a self-starting, implicite predictor-corrector method originally developed and widely used for gravitational N-body systems. The Hermite scheme takes the acceleration and its first time derivative to predict future position and velocity vectors from previous values. The beauty of the method relies on the fact that the second and third derivatives can be explicitely calculated from the acceleration and its first derivative alone. These are then used iteratively to correct the object's state vector, yielding an integration method with fourth-order global error. The method can be used with constant or variable timesteps. For constant timesteps the Hermite integrator is time-symmetric, and shows no secular error in the semi-major axis and eccentricity. The code can integrate a large number of objects in parallel, with either shared or individual timesteps. This can be applied for predicting future states of a catalogue of space objects, or to propagate an object's state uncertainty (covariance) in a realistic manner.

Key words: space debris; astrodynamics; numerical integration method.

1. INTRODUCTION

DLR's Institute of Technical Physics is actively developing laser-based optical tracking methods to determine 3D positions of LEO space debris objects to within a few metres. For Space Situational Awareness applications like collision avoidance or re-entry analyses, any initial high-precision orbit needs to be propagated, taking into account the various gravitational and non-gravitational forces perturbing the object's orbit. A key prerequisite for that is an accurate, fast, and versatile integration method allowing the prediction of trajectories from initial conditions.

The integrator can be envisaged as the "beating heart of a dynamical simulation" [7]. Several numerical integration methods for the computation of satellite orbits have been developed, see [11] for an overview and a discussion on the advantages and disadvantages of the various methods. A special class of integrators are time-symmetric. They preserve first integrals (e.g. energy, angular momentum) for a conservative system [7]. Therefore, they are very useful for long-term simulations of dynamical systems. For a Keplerian orbit these integrators show no secular error in the semi-major axis and eccentricity when using constant timesteps.

Section 2 describes the Hermite integration scheme and the timestep selection. In Section 3 we assess the accuracy and performance of the Hermite scheme by comparing our results with the semi-analytical solution of the Kepler problem for various eccentricities. In Section 4 the applicablity of using the Hermite integrator for short-term propagation for $\sim$100 orbits is discussed. Finally, in Section 5 we show results from a long-term simulation covering 3 million orbits, corresponding to several hundreds years for LEO orbits.

2. HERMITE INTEGRATION SCHEME

The Hermite scheme is a direct integration method with predictor-corrector algorithm to solve the N-body problem. The method has found widespread applications for the numerical simulation of the dynamical evolution of many-body systems [8, 9, 5, 14, 2].

For an object the momentary acceleration $\boldsymbol{a}_0$ and the first derivative with respect to time $\dot{\boldsymbol{a}}_0$ are used to compute the future position $\boldsymbol{r}(t)$ and velocity $\boldsymbol{v}(t)$ at a desired time t from the corresponding instantaneous values $\boldsymbol{r}_0$ and $\boldsymbol{v}_0$ at time $t_0 < t$. In the first step, new position and velocity vectors are predicted for the next time step t by expanding $\boldsymbol{r}_0$ and $\boldsymbol{v}_0$ into Taylor series. The positive time difference $t - t_0$ is written as Δt.

$$\boldsymbol{r}_{\mathrm{p}}(t) = \boldsymbol{r}_0 + \boldsymbol{v}_0 \Delta t + \frac{1}{2}\boldsymbol{a}_0 \Delta t^2 + \frac{1}{6}\dot{\boldsymbol{a}}_0 \Delta t^3 \quad (1)$$

$$\boldsymbol{v}_{\mathrm{p}}(t) = \boldsymbol{v}_0 + \boldsymbol{a}_0 \Delta t + \frac{1}{2}\dot{\boldsymbol{a}}_0 \Delta t^2 \quad (2)$$

Higher-order derivatives of the acceleration have to be considered to improve the accuracy of the force polyno-

Proc. 7th European Conference on Space Debris, Darmstadt, Germany, 18–21 April 2017, published by the ESA Space Debris Office
Ed. T. Flohrer & F. Schmitz, (http://spacedebris2017.sdo.esoc.esa.int, June 2017)

mial. Making a Taylor series ansatz, one writes

$$\boldsymbol{a}(t) = \boldsymbol{a}_0 + \dot{\boldsymbol{a}}_0 \Delta t + \frac{1}{2}\boldsymbol{a}_0^{(2)} \Delta t^2 + \frac{1}{6}\boldsymbol{a}_0^{(3)} \Delta t^3 \quad (3)$$

$$\dot{\boldsymbol{a}}(t) = \dot{\boldsymbol{a}}_0 + \boldsymbol{a}_0^{(2)} \Delta t + \frac{1}{2}\boldsymbol{a}_0^{(3)} \Delta t^2 \ , \quad (4)$$

where $\boldsymbol{a}_0^{(n)}$ denotes the n-th derivative of $\boldsymbol{a}$ with respect to time evaluated at $t = t_0$. The quantities $\boldsymbol{a}_0$, $\dot{\boldsymbol{a}}_0$ are already known, while $\boldsymbol{a}(t)$ and $\dot{\boldsymbol{a}}(t)$ are evaluated using the predicted values for the particle's position $\boldsymbol{r}_\mathrm{p}$ and velocity $\boldsymbol{v}_\mathrm{p}$. We therefore designate the left-hand sides of Equations 3 and 4 with $\boldsymbol{a}_\mathrm{p}$ and $\dot{\boldsymbol{a}}_\mathrm{p}$, respectively. Solving the latter equation for $\boldsymbol{a}_0^{(2)}$ and substituting it in Equation 3, we obtain [9]:

$$\boldsymbol{a}_0^{(3)} = 12\frac{\boldsymbol{a}_0 - \boldsymbol{a}_\mathrm{p}}{\Delta t^3} + 6\frac{\dot{\boldsymbol{a}}_0 + \dot{\boldsymbol{a}}_\mathrm{p}}{\Delta t^2};$$

re-inserting this expression in Equation 3 yields

$$\boldsymbol{a}_0^{(2)} = -6\frac{\boldsymbol{a}_0 - \boldsymbol{a}_\mathrm{p}}{\Delta t^2} - 2\frac{2\dot{\boldsymbol{a}}_0 + \dot{\boldsymbol{a}}_\mathrm{p}}{\Delta t}.$$

That means the higher-order derivatives of the acceleration can be explicitly calculated in terms of $\boldsymbol{a}_\mathrm{p}$ and $\dot{\boldsymbol{a}}_\mathrm{p}$.

The predicted position and velocity of particle i can now be refined by expanding Equations 1 and 2 up to fourth order to corrected position and velocity:

$$\begin{aligned}
\boldsymbol{r}_\mathrm{c}(t) &= \boldsymbol{r}_\mathrm{p}(t) + \frac{1}{24}\boldsymbol{a}_0^{(2)} \Delta t^4 \\
&= \boldsymbol{r}_\mathrm{p}(t) - \frac{1}{4}(\boldsymbol{a}_0 - \boldsymbol{a}_\mathrm{p})\Delta t^2 - \frac{1}{12}(2\dot{\boldsymbol{a}}_0 + \dot{\boldsymbol{a}}_\mathrm{p})\Delta t^3 \\
\boldsymbol{v}_\mathrm{c}(t) &= \boldsymbol{v}_\mathrm{p}(t) + \frac{1}{6}\boldsymbol{a}_0^{(2)} \Delta t^3 + \frac{1}{24}\boldsymbol{a}_0^{(3)} \Delta t^4 \\
&= \boldsymbol{v}_\mathrm{p}(t) - \frac{1}{2}(\boldsymbol{a}_0 - \boldsymbol{a}_\mathrm{p})\Delta t - \frac{1}{12}(5\dot{\boldsymbol{a}}_0 + \dot{\boldsymbol{a}}_\mathrm{p})\Delta t^2,
\end{aligned}$$

where $\boldsymbol{a}_0^{(2)}$ and $\boldsymbol{a}_0^{(3)}$ have been substituted with the composite expressions derived previously. The remainder of the Taylor series is proportional to $\mathcal{O}(\Delta t^5)$. Taking the time derivative, we see that the error in the force calculation is of $\mathcal{O}(\Delta t^4)$. After re-grouping, the corrector reads:

$$\begin{aligned}
\boldsymbol{v}_\mathrm{c}(t) &= \boldsymbol{v}_0 + \frac{1}{2}(\boldsymbol{a}_0 + \boldsymbol{a}_\mathrm{p})\Delta t + \frac{1}{12}(\dot{\boldsymbol{a}}_0 - \dot{\boldsymbol{a}}_\mathrm{p})\Delta t^2 \\
\boldsymbol{r}_\mathrm{c}(t) &= \boldsymbol{r}_0 + \frac{1}{2}(\boldsymbol{v}_\mathrm{c} + \boldsymbol{v}_0)\Delta t + \frac{1}{12}(\boldsymbol{a}_0 - \boldsymbol{a}_\mathrm{p})\Delta t^2.
\end{aligned}$$

The sequence of, first, evaluation of the acceleration and its first derivative and, second, correction of the position and velocity can be iterated to increase the accuracy of the orbit integration. We typically use three (3) iterations.

The code can integrate an ensemble of objects in parallel, with either shared or individual timesteps. We use quantized so-called block timesteps, where the timestep lengths can only be negative powers of two $\Delta t_k = 2^{-k}$ [10]. This ensures that objects with the same timestep share the same simulation time. In this way, predictions and computations of forces and first derivatives can be done in parallel. Furthermore, this approach ensures co-eval output times, which is useful for generating ephemerides for a large sample of objects, e.g. a catalogue.

Hermite schemes with order sixth or eighth order have been developed for even higher precision [12].

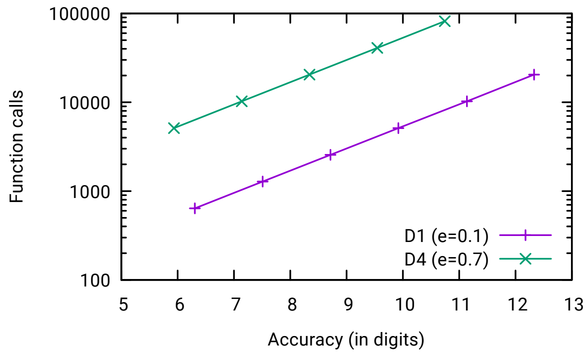

Figure 1. Performance diagram for the Hermite integration scheme, showing two test cases from [4].

3. TEST CASES

A set of test problems for (unperturbed) Kepler orbits have been defined in [4], with eccentricities ranging from 0.1 to 0.9 in steps of 0.2 (tests D1 to D5). All orbits are integrated for $20/2\pi \approx 3.18$ revolutions and the final state (two-dimensional position and velocity vectors) are compared to the analytical result found by iteratively solving Kepler's equations.

The numerical accuracy achieved at the end of an integration is defined as

$$\varepsilon = -\log\sqrt{\sum_{k=1}^{4}(x_k - \hat{x}_k)^2},$$

where x_k are the components of the state vector determined by numerical integration, and $\hat{x}_k$ the analytical reference orbit.

In Figure 1 we plot the numerical accuracy achieved with the fourth-order Hermite scheme for two test cases with eccentricities of $e = 0.1$ (D1) and $e = 0.7$ (D4). For the low-eccentricity case (nearly-circular orbit), an accuracy of $\sim$9 is obtained after about 2500 function calls, comparable to the RKF7 method of [3]. About 10 times more function calls are needed for the high-eccentricity orbit to reach the same accuracy.

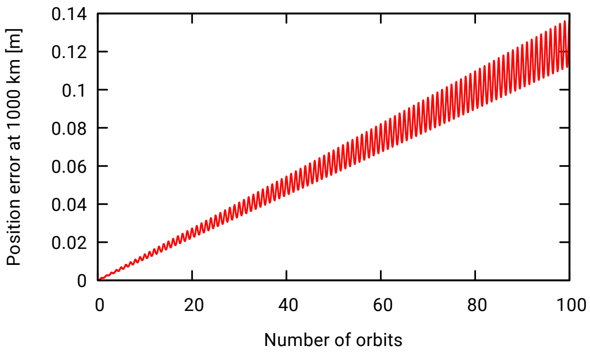

Figure 2. Errors in position due to the numerical method for an integration covering 100 orbits.

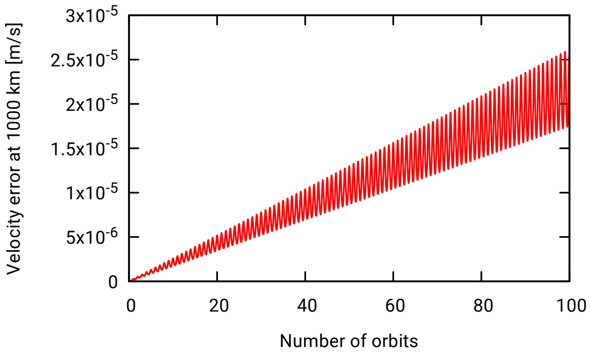

Figure 3. Errors in velocity due to the numerical method for an integration covering 100 orbits.

4. SHORT-TERM INTEGRATIONS

Propagation times of a few days and up to a week are relevant for SSA use cases like conjunction analysis, sensor tasking, etc. Here we demonstrate the applicability of the Hermite integration method for forecasting LEO orbits for these timescales. We chose a stop time of 200π, i.e. 100 orbits. For a typical RSO in LEO with $\sim$100 min orbital period the simulation covers $\sim$7 days.

The great majority of RSOs is on nearly circular orbits, with 90% of the objects having eccentricities < 0.1. Therefore, we selected an orbit with an eccentricity of $e = 0.1$, similar to test case D1 above. The evolution of the errors of position and velocity vectors for an orbit with semi-major axis $a = R_\mathrm{E} + 1000$ km are shown in Figures 2 and 3.

As is expected from the secular drift in the argument of pericentre [6], the errors in positions and velocity show a linear trend. The error in position after 100 orbits are well below one metre, proving that the Hermite integrator can be used for precise orbit determination based on laser-range measurements with metric accuracy. We found the velocity error to be $\sim$0.03 mm/sec. Both position and velocity errors oscillate with one orbital period with growing amplitude.

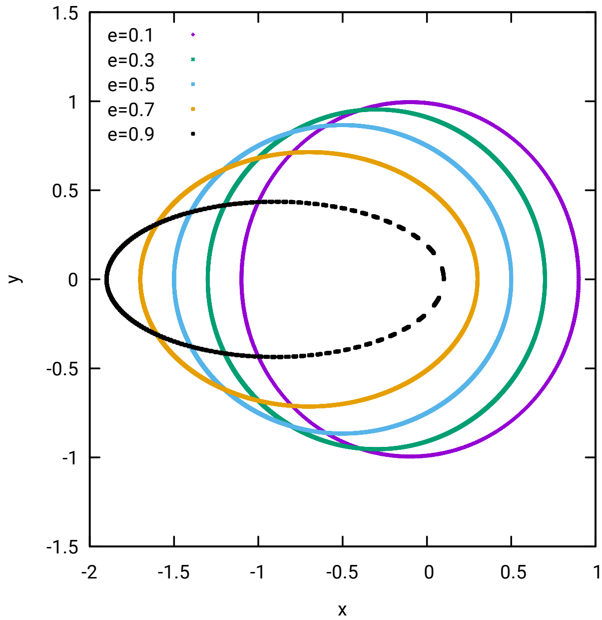

Figure 4. Position vectors in the orbital plane for the complete 3.2 million revolutions. Test orbits with initial eccentricities of 0.1, 0.3, 0.5, 0.7, and 0.9 are shown.

5. LONG-TERM INTEGRATIONS

Long-term integrations are required for analysing the orbital decay due to atmospheric drag, investigating resonant effects or chaotic motion, or studying space-debris populations. Here the superior properties of the Hermite integration scheme, that is conserving integral of motions as well as semimajor axis and eccentricity, will become apparent. We integrated the Kepler orbits D1 to D5 for 3.2 million revolutions, corresponding to $\sim$600 years for a LEO orbit.

Figure 4 displays the position vectors, illustrating that the overall orbital geometry is not changing over more than 3 million revolutions. Semimajor axes and eccentricities show no secular drift, and can be considered constant for all practical purposes. This can also be seen in the plot of the relative energy error $\Delta E/E_0$, see Figure 5. While the relative energy error undergoes periodic changes, no secular drift is present.

As discussed above the argument of pericentre ω undergoes a slow linear drift, cf. Figure 6. This is in contrast to high-order multistep integrators which generally have quadratic errors in the angle variables [6]. The error grows with eccentricity.

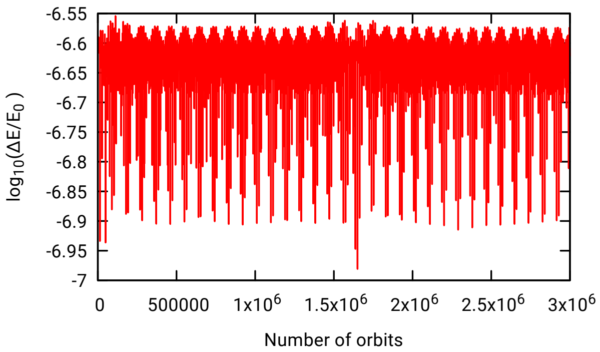

Figure 5. Change of the relative energy error over the integration time for a set of 5 objects on D1 to D5 orbits.

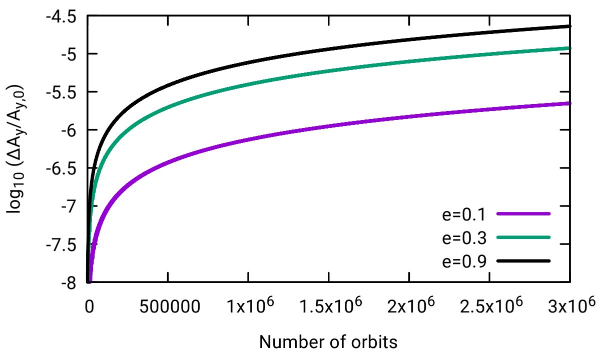

Figure 6. Relative error of the y-component of the Laplace-Runge-Lenz vector.

6. SUMMARY

We have demonstrated that the Hermite integration scheme is a very useful numerical method for orbit propagation. Especially due to its time-symmetry the integrator has several desirable properties that make it highly useful for long-term simulation of orbital dynamics up to several millions of revolutions. For a conservative system, energy and angular momentum show no secular errors. As a consequence, both semimajor axis and eccentricity of an object are not drifting away from their initial values.

The Hermite scheme provides excellent accuracy on the propagated state vectors for short-term integrations, which are important for several applications and use cases in the domain of Space Situational Awareness (uncertainty propagation, conjunction analysis, or re-entry predictions). For example, a 7-day propagation of a typical LEO orbit results in a numerical position error below 1 metre.

The code can integrate an ensemble of objects in parallel, with either shared or individual timesteps. It can therefore be applied to propagate a catalogue of space objects and/or to perform realistic uncertainty propagation via Monte-Carlo or sigma-point methods.

REFERENCES

1. Aarseth J. S., (2003), *Gravitational N-Body Simulations*, Cambridge University Press
2. Ertel S., Wolf S., Rodmann J., (2012), A&A, **544**, A61
3. Fehlberg E., (1968), Technical Report NASA TR R-287
4. Hull T. E., Enright W. H., Fellen B. M. et al., (1972), SIAM Journal on Numerical Analysis, **9**(4), 603–637
5. Kokubo E., Yoshinaga K., Makino J., (1998), MNRAS, **297**, 1067–1072
6. Kokubo E., Makino J., (2004), PASP, **56**, 861–868
7. Leimkuhler B., Reich S., (2004), *Simulating Hamiltonian Dynamics*, Cambridge University Press
8. Makino J., (1991), ApJ, **369**, 200–212
9. Makino J., Aarseth S. J., (1992), PASP, **44**, 141–151
10. McMillan S. L. W., (1986), in *The Use of Supercomputers in Stellar Dynamics*, Springer, 156
11. Montenbruck O., Gill E., (2012), *Satellite Orbits*, Springer
12. Nitadori K., Makino J., (2008), New Astronomy, **13**, 498–507
13. Quinlan G. D., Tremaine S., (1990), AJ, **104**, 4
14. Rodmann J., (2006), *Dust in Circumstellar Disks*, Ph.D. thesis